Article

Chinese Science Bulletin

SPECIAL ISSUE
Bulk Metallic Glasses

December 2011 Vol.56 No.36: 3902–3907
doi: 10.1007/s11434-011-4842-z

Revisiting Al-Ni-Zr bulk metallic glasses using the 'cluster-resonance' model

LI FengWei, QIANG JianBing*, WANG YingMin, WANG Qing, DONG XingLong & DONG Chuang

Key Laboratory of Materials Modification of Ministry of Education, Dalian University of Technology, Dalian 116024, China

Received June 16, 2011; accepted September 22, 2011

Six series of alloys, namely, $Ni_3Zr_6Al_x$, $Ni_3Zr_7Al_x$, $Ni_4Zr_9Al_x$, $Ni_3Zr_8Al_x$, $Ni_3Zr_9Al_x$ and $Ni_3Zr_{10}Al_x$ (x=1, 1.5, 2, 3) were designed in this work and the bulk metallic glass (BMG) formation of these compositions was investigated by copper mold suction casting. A centimeter-scale BMG sample was obtained for the $Ni_4Zr_9Al_2$ ($Al_{13.3}Ni_{26.7}Zr_{60}$ in atomic percent) composition. The thermal glass parameters for this BMG were determined to be ΔT_x = 68 K, T_{rg} = 0.579, and γ_m = 0.689. Using the 'cluster-resonance' model for glass formation an optimal BMG composition was determined using the cluster formula $[Ni_3Zr_9](Al_2Ni_1)$.

bulk metallic glass, glass-forming ability, Al-Ni-Zr, cluster formula

Citation: Li F W, Qiang J B, Wang Y M, et al. Revisiting Al-Ni-Zr bulk metallic glasses using the 'cluster-resonance' model. Chinese Sci Bull, 2011, 56: 3902–3907, doi: 10.1007/s11434-011-4842-z

To date, a large variety of bulk metallic glasses (BMGs) have been discovered [1], and Zr-based BMGs are among the most promising structural materials. This is because they exhibit a combination of high strength, toughness and anti-corrosion properties [1,2]. Many multi-component Zr-based BMG systems exist such as Al-Cu-Ni-Zr [3], Be-Cu-Ni-Ti-Zr [4], Al-Cu-Ni-Nb(Ti)-Zr [5,6] and Ag-Al-Cu-Zr [7]. These complex alloys are based on the basic ternary systems of Al-*TM*-Zr (*TM* = Ni, Co, Cu) together with specific alloying substitutes [5,7,8]. A rationalization of the glass-forming abilities (GFAs) of Al-TM-Zr alloys is desirable to quantify complex BMG compositions. Disagreements exist with regard to experimental accounts of the GFA for fundamental ternary systems [9–11]. This study is devoted to a reexamination of the GFAs of Al-Ni-Zr alloys.

We first use the 'cluster-plus-glue-atom' model [12,13] for BMG composition design. This model presents a semi-phenomenological treatment of a BMG structure. An atomic cluster of specific topology, chemical composition and glue structure were used to establish the statistical composition of a BMG system. An ideal BMG assumes universal cluster formulae such as $[\text{cluster}]_1(\text{glue atoms})_x$, with x=1 or 3 [13,14]. To determine the structural stability of the model structure we recently proposed a 'cluster-resonance' model by taking the coupling of long-range Friedel oscillations of valence electrons with the pair correlation function into consideration [15]. The composition design of Al-Ni-Zr BMG alloys is incorporated into the model that follows.

1 The 'cluster-resonance' model and composition design

According to Häussler et al. [16] the static atomic structure of an ideal amorphous state is in resonance with the long-range Friedel oscillations of valence electrons. The resonance results in spherical periodicity as shown by the peak (shell) oscillation with a certain period in the pair correlation function of an ideal amorphous state. The spherical periodicity gives an oscillation wavelength (λ_{Fr}) in the form of

*Corresponding author (email: qiang@dlut.edu.cn)

$$r_n = \left(n + \frac{1}{4}\right)\lambda_{\mathrm{Fr}}, \tag{1}$$

where r_n is the radius of the nth shell centered by any atom and

$$\lambda_{\mathrm{Fr}} = \frac{2\pi}{K_{\mathrm{P}}}, \tag{2}$$

where K_{p} is the wave vector of the reciprocal space. The resonance condition for an ideal amorphous state yields a matching relation $K_{\mathrm{p}} = 2k_{\mathrm{F}}$ where k_{F} is the Fermi momentum. Therefore,

$$k_{\mathrm{F}} = \frac{K_{\mathrm{P}}}{2} = \frac{\pi}{\lambda_{\mathrm{Fr}}} = \frac{1.25\pi}{r_1}, \tag{3}$$

with which the effective electron concentration (e/a) for an ideal amorphous state can be obtained:

$$\frac{e}{a} = \frac{1.25^3\pi}{3} \times \frac{1}{\rho_{\mathrm{a}} \cdot r_1^3}, \tag{4}$$

where r_1 is the radius of the nearest-neighbor shell of the cluster and ρ_{a} is the number of atoms per unit volume. The determination of the atomic cluster structure is, therefore, required for the composition design of Al-Ni-Zr BMGs.

Although not entirely convincing the existing experimental evidence discloses a local structure similarity between metallic glasses and their crystalline counterparts [17–19]. A strongly negative mixing enthalpy exists between Ni and Zr at a 1∶1 atomic ratio. We considered Ni-Zr atomic clusters in the known crystalline phases of the Al-Ni-Zr system. Intermetallic phases of Al_2NiZr_6 ($InMg_2$ type), $NiZr_2$ (Al_2Cu type) and metastable cF-$NiZr_2$ ($NiTi_2$ type) are known crystallization products of Zr-based Al-Ni-Zr BMGs [20,21]. In the different structures three Ni-centered clusters, namely, a CN11 Ni-Ni_2Zr_9 capped trigonal prism (Figure 1(a)), a CN10 Ni-Ni_2Zr_8 octahedral antiprism (Figure 1(b)) and a CN12 Ni-Ni_3Zr_9 icosahedron (Figure 1(c)) have been identified. Here '–' is used to distinguish the central atom (before –) from shell atoms (after –). A binary NiZr phase of BCr-type is also considered and it consists of an atomic cluster of a CN9 Ni-Ni_2Zr_7 Archimedes octahedral antiprism (Figure 1(d)). Within the framework of the 'cluster-plus-glue-atom' model, atomic clusters that preserve the same topological configurations that are of a statistically averaged composition serve as the chair tilings of an ideal amorphous structure pattern.

In a ternary composition diagram, the 'cluster-plus-glue-atom' model is embodied by a cluster line, which links an atomic cluster composition to the glue atom [14]. Therefore, four cluster lines in the forms of Ni_3Zr_9-Al, Ni_3Zr_8-Al, Ni_4Zr_9-Al and Ni_3Zr_7-Al were established by linking the respective atomic clusters to the glue atom Al in the Al-Ni-Zr system. Another two composition lines, Ni_3Zr_6-Al and Ni_3Zr_{10}-Al, were also considered for comparison. An experimental investigation into GFAs was performed for the six series of alloys shown in Figure 2: $Ni_3Zr_9Al_x$, $Ni_3Zr_8Al_x$, $Ni_4Zr_9Al_x$, $Ni_3Zr_7Al_x$, $Ni_3Zr_6Al_x$ and $Ni_3Zr_{10}Al_x$ (x=1, 1.5, 2 and 3).

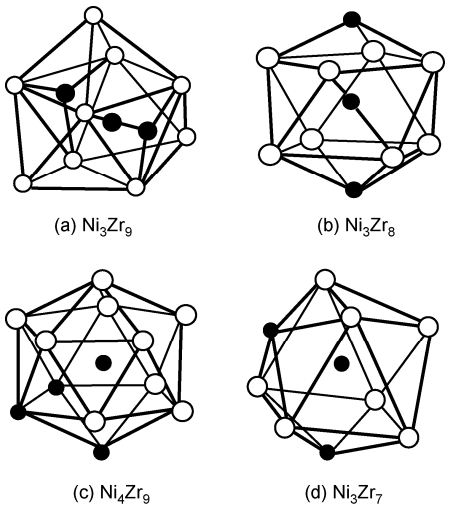

Figure 1 Schematics of the Ni-Zr clusters. (a) Ni_3Zr_7, (b) Ni_3Zr_8, (c) Ni_4Zr_9 and (d) Ni_3Zr_9. Dark circles represent Ni atoms and white circles represent Zr atoms.

2 Experimental

Ingots for the designed alloys along with a reference composed of $Al_{15}Ni_{20}Zr_{60}$ were prepared by arc melting the mixtures of the elemental constituents under an argon atmosphere. The purities of Zr, Ni and Al are 99.99 wt.%. The ingots were remelted three times to ensure composition homogeneity. The overall weight loss was less than 0.1% after arc melting. Alloy rods of various diameters from 3 to

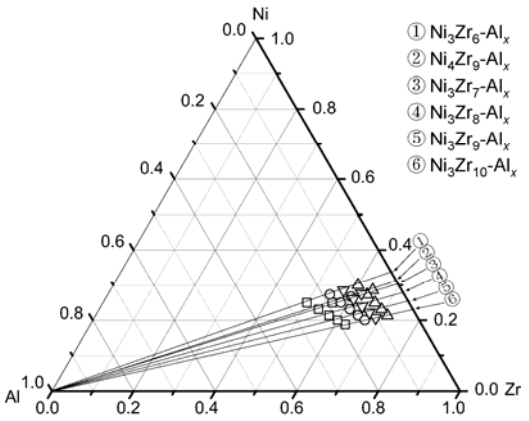

Figure 2 Six composition lines in the Al-Ni-Zr ternary system with experimental compositions marked by the symbols △, ▽, ○, □, which indicate the compositions of the composition lines as x=1, 1.5, 2, 3, respectively.

10 mm and 40 mm long were made by copper mold suction casting. A phase identification of the alloy rods were carried out using X-ray diffractometry (XRD, D8 Discover, Bruker AXS GmbH, Germany) with Cu-Kα radiation (λ=0.15406 nm). A TA-Q100 differential scanning calorimeter (DSC, TA-Q100, TA Instruments, USA) and a TA-Q600 SDT differential thermal analysis instrument (DTA, TA-Q600, TA Instruments) were employed to examine the glass transition temperature (T_g), the onset crystallization temperature (T_x), the onset melting temperature (T_m) and the liquidus temperature (T_l) of the BMG samples at a constant heating rate of 20 K/min. The mass densities of the glassy rods were measured using the Archimedes water immersion method.

3 Results and discussion

3.1 BMG formation

Figure 3(a) shows XRD results of the 3 mm diameter as-cast rods. All the rods except for $Ni_3Zr_6Al_3$ appear to be amorphous. The amorphous structure is retained in the 5 mm rod diameter samples of $Ni_3Zr_6Al_2$, $Ni_3Zr_7Al_x$ (x=1, 1.5, 2, 3), $Ni_4Zr_9Al_x$ (x=2, 3), $Ni_3Zr_8Al_x$ (x=1, 1.5, 2, 3), $Ni_3Zr_9Al_x$ (x=2, 3) and $Ni_3Zr_{10}Al_x$ (x=2, 3) (Figure 3(b)). For the 8 mm diameter cases, the $Ni_3Zr_7Al_x$ (x=1.5, 2, 3), $Ni_4Zr_9Al_x$ (x=2, 3) and $Ni_3Zr_8Al_x$ (x=1.5, 2, 3) alloys are fully amorphous (Figure 3(c)). $Ni_4Zr_9Al_2$ ($Al_{13.3}Ni_{26.7}Zr_{60}$, at%) was found to have the best BMG-forming ability, which is associated with its critical diameter of up to 10 mm (Figure 3(d)). The other alloys, including $Al_{15}Ni_{20}Zr_{60}$, were partially crystallized under the slowest cooling rate. The quantized experimental GFA evidence is summarized in Figure 4. The critical BMG diameter decreases drastically from 8 to 3 mm with a decrease in Al content around $Ni_4Zr_9Al_2$. Li et al. [11] reported a critical diameter of 15 mm for $Al_{15}Ni_{20}Zr_{60}$ glass in a pour-casting experiment. Our casting experiment, however, indicates that its GFA is inferior to that of $Ni_4Zr_9Al_2$.

3.2 Thermal glass parameters

The thermal glass properties of the Al-Ni-Zr BMG samples were examined with 3-mm diameter samples and $Ni_3Zr_6Al_3$ (2 mm critical BMG diameter) was excluded. All the DSC

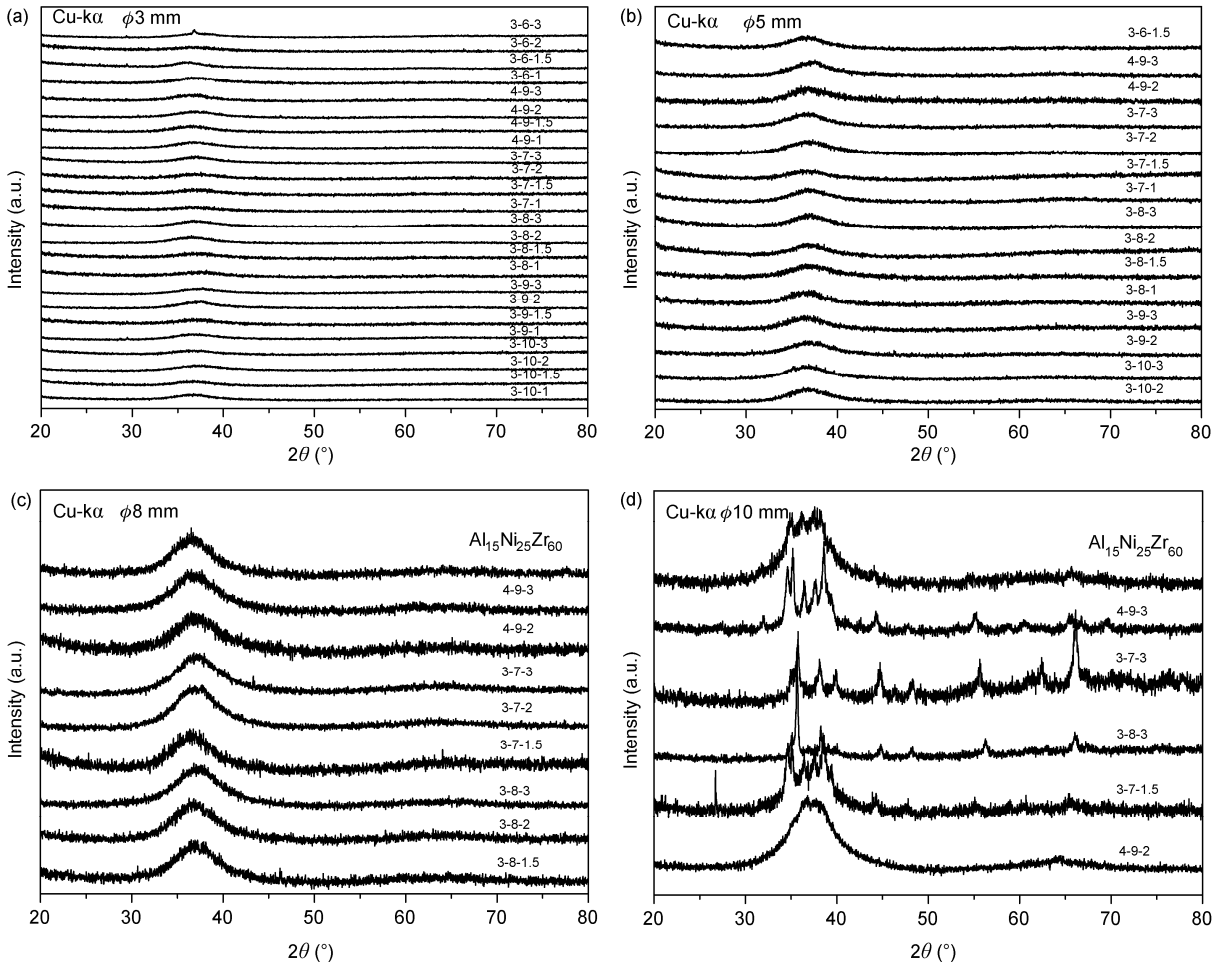

Figure 3 XRD diffraction patterns of the suction-cast rods with diameters of (a) 3 mm, (b) 5 mm, (c) 8 mm and (d) 10 mm. The alloy composition is denoted by a specific number series of "*z*-*y*-*x*", e.g., "3-6-3" represents the Ni_3Zr_6-Al_3 alloy.

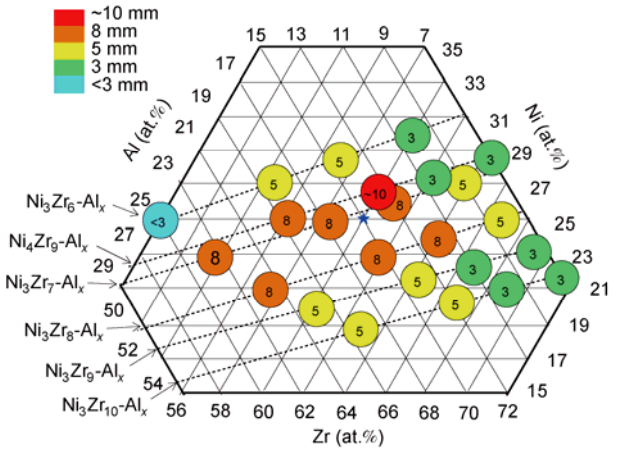

Figure 4 Critical sizes of glass formation along the six composition lines. The blue star represents the reference $Al_{15}Ni_{25}Zr_{60}$ and its critical size is also 8 mm under the present casting conditions.

and DTA curves are given in Figure 5 from which T_g, T_x, T_m and T_l were determined following common criteria. The GFA indicators, e.g., ΔT_x ($=T_x-T_g$) [22], T_{rg} ($=T_g/T_l$) [23] and γ_m ($=(2T_x-T_g)/T_l$) [24] were calculated using the obtained experimental thermal glass data. The data are summarized in Table 1. The DSC curves are characterized by a distinct glass transition followed by crystallization exothermic peaks. The crystallization behavior evidently changes with composition as signaled by the different amounts of exothermic peaks. The DTA curves reveal multiple melting peaks while T_m is nearly the same for most of the Al-Ni-Zr alloys.

A special phenomenon as observed from the DSC curves is that some of BMG series like $Ni_3Zr_6Al_x$ (x=1.5, 2), $Ni_4Zr_9Al_x$ (x=2, 3), $Ni_3Zr_7Al_x$ (x=2, 3), $Ni_3Zr_8Al_3$, $Ni_3Zr_9Al_3$, $Ni_3Zr_{10}Al_3$ and $Al_{15}Ni_{25}Zr_{60}$ are quite weird, while others look normal. It has to noted that all the DSC curves were obtained under the same DSC experimental conditions. The unusual phenomena are confirmed by our repeated DSC experiments carefully, which imply that the irregular peaks are the intrinsic responses of the materials rather than from the instrument problem. We suppose that the weird DSC curves may be relevant to the thermal-conduct properties of the BMG alloys and will be the subject of our future research.

Figure 6 shows the composition dependence of the GFA indicators of these BMG alloys. The ΔT_x and γ_m values peak in the vicinity of $Ni_4Zr_9Al_2$ while T_{rg} has a maximum value at $Ni_3Zr_6Al_2$. The DTA melting behavior of $Ni_3Zr_6Al_2$ indicates that it is near to a eutectic composition. The GFA indicator values are ΔT_x=68 K, T_{rg}=0.579 and γ_m=0.689 for $Ni_4Zr_9Al_2$ and ΔT_x=68 K, T_{rg}=0.568 and γ_m=0.676 for $Al_{15}Ni_{25}Zr_{60}$, respectively.

3.3 *e/a* and cluster formulae

The $Ni_4Zr_9Al_2$ ($Al_{13.3}Ni_{26.7}Zr_{60}$) alloy gave the best GFA in the casting experiment. However, the number ratio of the atomic cluster and the glue atoms does not satisfy the universal cluster formulae of $[cluster]_1(glue\ atoms)_x$, with x=1 or 3. The Ni_4Zr_9 cluster, therefore, cannot be viewed as a fundamental atomic cluster considering the model structure. The atomic cluster, to be feasible as a model structure, has to adhere to structural stability considerations. The cluster-resonance model was then employed to identify the model cluster from the four known clusters, namely, Ni_3Zr_9, Ni_3Zr_8, Ni_4Zr_9 and Ni_3Zr_7, with which the cluster formulae for the $Al_{13.3}Ni_{26.7}Zr_{60}$ BMG was eventually determined.

As shown in Section 2, the effective *e/a* value for an ideal amorphous structure can be determined from eq. (4) when r_1 and ρ_a are known. As for the Ni_3Zr_9 atomic cluster, $r_{1\text{-}Ni3Zr9}$ = 0.29058 nm was obtained by averaging the distances between the first-neighbor shell atoms (Ni_2Zr_9) and the central atom Ni, which was abstracted from the structural

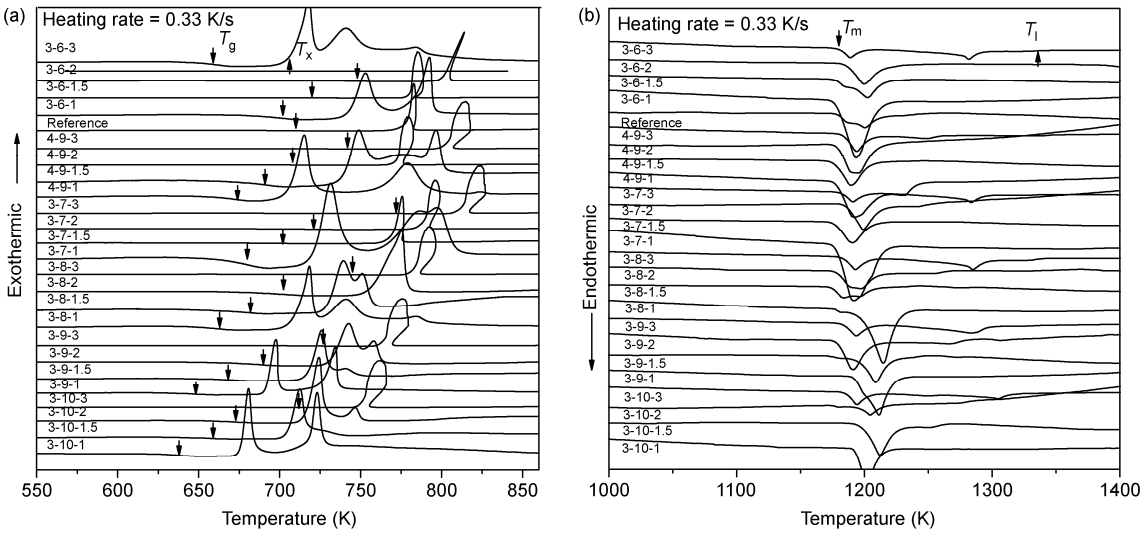

Figure 5 (a) DSC and (b) DTA curves of the Al-Ni-Zr glassy alloys. The "reference" represents the $Al_{15}Ni_{25}Zr_{60}$ glassy sample.

Table 1 Summary of the thermal properties of the ternary Al-Ni-Zr glassy alloys

Designed compositions	Compositions (at.%)	T_g (K)	T_x (K)	T_m (K)	T_l (K)	ΔT_x (K)	T_g/T_l	γ_m
$Ni_3Zr_{10}Al_1$	$Al_{7.1}Ni_{21.4}Zr_{71.4}$	638	676	1193	1223	38	0.522	0.584
$Ni_3Zr_{10}Al_{1.5}$	$Al_{10.3}Ni_{20.7}Zr_{69}$	659	704	1199	1263	45	0.522	0.593
$Ni_3Zr_{10}Al_2$	$Al_{13.3}Ni_{20}Zr_{66.7}$	673	716	1174	1307	43	0.515	0.581
$Ni_3Zr_{10}Al_3$	$Al_{18.8}Ni_{18.7}Zr_{62.5}$	712	751	1185	1319	39	0.540	0.599
$Ni_3Zr_9Al_1$	$Al_{7.7}Ni_{23.1}Zr_{69.2}$	649	691	1192	1233	42	0.526	0.594
$Ni_3Zr_9Al_{1.5}$	$Al_{11.1}Ni_{22.2}Zr_{66.7}$	669	717	1172	1278	48	0.523	0.599
$Ni_3Zr_9Al_2$	$Al_{14.3}Ni_{21.4}Zr_{64.3}$	690	731	1179	1316	41	0.524	0.587
$Ni_3Zr_9Al_3$	$Al_{20}Ni_{20}Zr_{60}$	727	765	1184	1319	38	0.542	0.598
$Ni_3Zr_8Al_1$	$Al_{8.3}Ni_{22.5}Zr_{66.7}$	663	710	1199	1236	47	0.536	0.612
$Ni_3Zr_8Al_{1.5}$	$Al_{12}Ni_{24}Zr_{64}$	682	729	1174	1283	47	0.532	0.605
$Ni_3Zr_8Al_2$	$Al_{15.4}Ni_{23.1}Zr_{61.5}$	703	758	1178	1266	55	0.555	0.642
$Ni_3Zr_8Al_3$	$Al_{21.4}Ni_{21.4}Zr_{57.2}$	745	784	1183	1342	39	0.557	0.615
$Ni_3Zr_7Al_1$	$Al_{9.1}Ni_{27.3}Zr_{63.6}$	680	721	1178	1220	41	0.557	0.625
$Ni_3Zr_7Al_{1.5}$	$Al_{13}Ni_{26}Zr_{61}$	702	770	1176	1263	68	0.556	0.663
$Ni_3Zr_7Al_2$	$Al_{16.7}Ni_{25}Zr_{58.3}$	721	789	1185	1289	68	0.559	0.665
$Ni_3Zr_7Al_3$	$Al_{23.1}Ni_{23.1}Zr_{53.8}$	772	813	1182	1338	41	0.578	0.639
$Ni_4Zr_9Al_1$	$Al_{7.1}Ni_{28.6}Zr_{64.3}$	673	706	1178	1244	33	0.541	0.594
$Ni_4Zr_9Al_{1.5}$	$Al_{10.3}Ni_{27.6}Zr_{62.1}$	691	739	1176	1239	48	0.558	0.635
$Ni_4Zr_9Al_2$	$Al_{13.3}Ni_{26.7}Zr_{60}$	707	775	1179	1222	68	0.579	0.689
$Ni_4Zr_9Al_3$	$Al_{18.8}Ni_{25}Zr_{56.2}$	742	804	1184	1336	62	0.550	0.642
$Ni_3Zr_6Al_1$	$Al_{10}Ni_{30}Zr_{60}$	702	743	1178	1219	41	0.576	0.643
$Ni_3Zr_6Al_{1.5}$	$Al_{14.3}Ni_{28.6}Zr_{57.1}$	720	780	1177	1280	60	0.563	0.656
$Ni_3Zr_6Al_2$	$Al_{18.2}Ni_{27.3}Zr_{54.5}$	748	800	1186	1252	52	0.597	0.681
$Ni_3Zr_6Al_3$	$Al_{25}Ni_{25}Zr_{60}$	659	710	1180	1348	51	0.493	0.570
Reference	$Al_{15}Ni_{25}Zr_{60}$	710	778	1177	1251	68	0.568	0.676

data of the hP-Al_2NiZr_6 phase. Similarly, $r_{1\text{-}Ni3Zr8}$ = 0.2734 nm was derived from the $NiZr_2$ phase (Al_2Cu type); $r_{1\text{-}Ni4Zr9}$ = 0.28603 nm was calculated using the lattice constants of the metastable cF-$NiZr_2$ phase (a=1.2282 nm) [21]; and $r_{1\text{-}Ni3Zr7}$ = 0.2688 nm was obtained from the NiZr phase (BCr-type).

The atomic density ρ_a (number of atoms per unit volume) for the $Ni_4Zr_9Al_2$ BMG can be determined using

$$\rho_a = \frac{N_A \rho}{M_A}, \tag{5}$$

where $M_A = \left(\sum_i C_i M_i\right) \Big/ Z$ is the average mole-mass of the alloy, M_i is the atomic mass of element i, N_A the Avogadro constant and ρ the mass density, which can either be measured or derived from our structure model [25]. The mass density ρ and the mole-mass M_A of $Ni_4Zr_9Al_2$ ($Al_{13.3}Ni_{26.7}Zr_{60}$) are 6.49 g cm^{-3} and 73.98 g mol^{-1}, respectively. We then obtain ρ_a = 52.809 nm^{-3} for the BMG. Using ρ_a, r_1 and eq. (4) the e/a values were found to be 1.578, 1.895, 1.655 and 1.994 for the ideal amorphous structures of the alloy and this was established by assuming model clusters of Ni_3Zr_9, Ni_3Zr_8, Ni_4Zr_9 and Ni_3Zr_7, respectively.

The effective e/a and number of atoms (Z) in the unit cluster formula follow the relationship [25]:

$$\frac{e}{a} = 23.614 \times \frac{1}{Z}, \tag{6}$$

The Z values of 15.0, 12.5, 14.3 and 11.8 that were obtained from the relationship correspond to atomic clusters of Ni_3Zr_9, Ni_3Zr_8, Ni_4Zr_9 and Ni_3Zr_7. By subtracting the atomic numbers of a cluster from Z the respective glue atom numbers are determined as 3, 1.5, 1.3 and 1.8 for the different model clusters. The Ni_3Zr_9 cluster was the only cluster that adequately satisfied the universal cluster formulae. The best BMG composition ($Al_{13.3}Ni_{26.7}Zr_{60}$) is described by the cluster formula $[Ni_3Zr_9](Al_2Ni)$ in which two Al and one Ni are the glue atoms. It is worth mentioning that the Ni_3Zr_9 cluster is derived from one of its crystalline counterparts, the hP-Al_2NiZr_6 phase.

4 Conclusion

The GFAs of Al-Ni-Zr alloys were re-examined using the cluster-plus-glue-atom model. A centimeter scale BMG alloy of $Ni_4Zr_9Al_2$ = $Al_{13.3}Ni_{26.7}Zr_{60}$ was found in our mold casting experiment and it is associated with a cluster formula of $[Ni_3Zr_9](Al_2Ni)$. The validity of the cluster-plus-glue-atom models for BMG composition design was verified in the Al-Ni-Zr system.

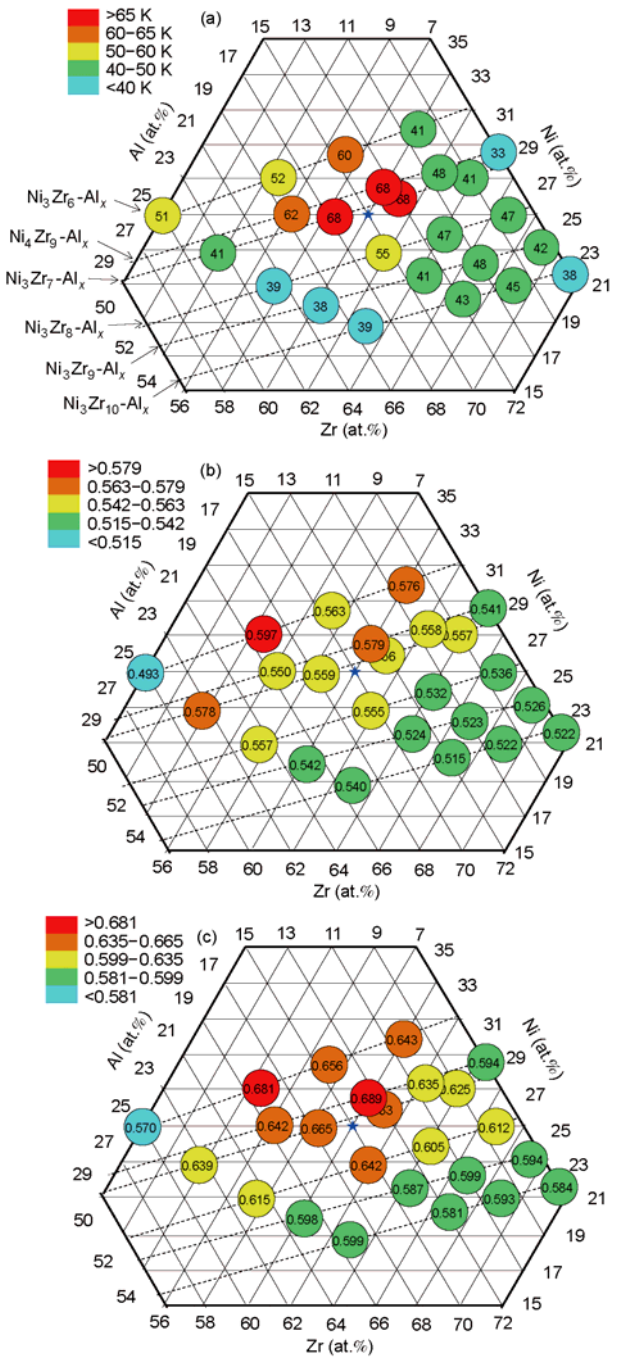

Figure 6 Composition dependence of (a) ΔT_x, (b) T_{rg} and (c) γ_m for the Al-Ni-Zr glassy alloys. The blue star in each diagram represents the reference $Al_{15}Ni_{25}Zr_{60}$ and its ΔT_x, T_{rg} and γ_m values are 68 K, 0.568 and 0.676, respectively.

This work was supported by the National Natural Science Foundation of China (51041011 and 50901012) and the National Basic Research Priorities Program of China (2007CB613902).

1 Wang W H, Dong C, Shek C H. Bulk metallic glasses. Mater Sci Eng R, 2004, 44: 45–89
2 Inoue A. Stabilization of metallic supercooled liquid and bulk amorphous alloys. Acta Mater, 2000, 48: 279–306
3 Inoue A, Zhang T, Nishiyama N, et al. Preparation of 16 mm diameter rod of amorphous $Zr_{65}Al_{7.5}Ni_{10}Cu_{17.5}$. Mater Trans, 1993, 34: 1234–1237
4 Peker A, Johnson W L. A highly processable metallic glass: $Zr_{41.2}Ti_{13.8}Cu_{12.5}Ni_{10.0}Be_{22.5}$. Appl Phys Lett, 1993, 63: 2342–2344
5 Inoue A, Shibata T, Zhang T. Effect of additional elements on glass transition behavior and glass formation tendency of Zr-Al-Ni-Cu alloys. Mater Trans, 1995, 36: 1420–1426
6 Hays C C, Schroers J, Geyer U, et al. Glass forming ability in the Zr-Nb-Ni-Cu-Al bulk metallic glasses. Mater Sci Forum, 2000, 343: 103–108
7 Zhang G Q, Jiang Q K, Chen L Y, et al. Synthesis of centimeter-size Ag-doped Zr-Cu-Al metallic glasses with large plasticity. J Alloys Comp, 2006, 424: 176–178
8 Zhang T, Inoue A, Masumoto T. Amorphous Zr-Al-*TM* (*TM*=Co, Ni, Cu) alloys with significant supercooled liquid region of over 100 K. Mater Trans, 1991, 32: 1005–1010
9 Wang Y M, Shek C H, Qiang J B, et al. The *e/a* factor governing the formation and stability of $(Zr_{76}Ni_{24})_{1-x}Al_x$ bulk metallic glasses. Scrip Mater, 2003, 48: 1525–1529
10 Jing Q, Zhang Y, Wang D, et al. A study of the glass forming ability in ZrNiAl alloys. Mater Sci Eng A, 2006, 441: 106–111
11 Li Y H, Zhang W, Dong C, et al. Formation and mechanical properties of Zr-Ni-Al glassy alloys with high glass-forming ability. Intermetallics, 2010, 18: 1851–1855
12 Dong C, Wang Q, Qiang J B, et al. From clusters to phase diagrams: Composition rules of quasicrystals and bulk metallic glasses. J Phys D: Appl Phys, 2007, 40: 273–291
13 Dong C, Qiang J B, Wang Y M, et al. Cluster-based composition rule for stable ternary quasicrystals in Al-(Cu, Pd, Ni)-TM systems. Phil Mag, 2006, 86: 263–274
14 Wang Q, Dong C, Qiang J B, et al. Cluster line criterion and Cu-Zr-Al bulk metallic glass formation. Mater Sci Eng A, 2007, 449-451: 18–23
15 Han G, Qiang J B, Wang Q, et al. Composition formulae of ideal metallic glasses and their relevant eutectics established by a cluster-resonance model. Phi Mag, 2011, 91: 2404–2418
16 Häussler P, Barzola-Quiquia J, Haberkern R, et al. On fundamental structure forming processes. In: Trebin H R, ed. Quasicrystals: Structure and Physical Properties. Weinheim, Germany: Wiley-VCH, 2003. 289
17 Gaskell P H. New structural model for transition metal-metalloid glasses. Nature, 1978, 276: 484–485
18 Miracle D B. Efficient local packing in metallic glasses. J Non-Cryst Solids, 2004, 342: 89–96
19 Liu X J, Chen G L, Liu C T. Correlation between primary phases and atomic clusters in a Zr-based metallic glass. J Appl Phys, 2010, 108: 123516
20 Li C F, Saida J, Matsushida M, et al. Crystallization process of $Zr_{60}Ni_{25}Al_{15}$ amorphous alloy. Mater Lett, 2000, 44: 80–86
21 El-Eskandarany M S, Saida J, Inoue A. Structural and calorimetric evolutions of mechanically induced solid-state devitrificated $Zr_{60}Ni_{25}Al_{15}$ glassy alloy powder. Acta Mater, 2003, 51: 1481–1492
22 Inoue A, Zhang W, Zhang T, et al. Formation and mechanical properties of Cu-Hf-Ti bulk glassy alloys. J Mater Res, 2001, 16: 2836–2844
23 Turnbull D. Under what conditions can a glass be formed? Contempt Phys, 1969, 10: 473–488
24 Du X H, Huang J C, Liu C T, et al. New criterion of glass forming ability for bulk metallic glasses. J Appl Phys, 2007, 101: 86108
25 Han G, Qiang J B, Li F W, et al. The *e/a* values of ideal metallic glasses in relation to cluster formulae. Acta Mater, 2011, 59: 5917–5923